

# Hydrodynamic simulations of self-phoretic microswimmers

Mingcheng Yang,<sup>1,2,\*</sup> Adam Wysocki,<sup>1</sup> and Marisol Ripoll<sup>1,†</sup>

<sup>1</sup>*Theoretical Soft-Matter and Biophysics, Institute of Complex Systems,  
Forschungszentrum Jülich, 52425 Jülich, Germany*

<sup>2</sup>*Beijing National Laboratory for Condensed Matter Physics and Key Laboratory of Soft Matter Physics,  
Institute of Physics, Chinese Academy of Sciences, Beijing 100190, China*

(Dated: February 24, 2022)

A mesoscopic hydrodynamic model to simulate synthetic self-propelled Janus particles which is thermophoretically or diffusiophoretically driven is here developed. We first propose a model for a passive colloidal sphere which reproduces the correct rotational dynamics together with strong phoretic effect. This colloid solution model employs a multiparticle collision dynamics description of the solvent, and combines potential interactions with the solvent, with stick boundary conditions. Asymmetric and specific colloidal surface is introduced to produce the properties of self-phoretic Janus particles. A comparative study of Janus and microdimer phoretic swimmers is performed in terms of their swimming velocities and induced flow behavior. Self-phoretic microdimers display long range hydrodynamic interactions and can be characterized as pullers or pushers. In contrast, Janus particles are characterized by short range hydrodynamic interactions and behave as neutral swimmers. Our model nicely mimics those recent experimental realization of the self-phoretic Janus particles.

PACS numbers: 66.10.cd, 87.17.Jj, 05.70.Ln, 02.70.Ns

## I. INTRODUCTION

Synthetic microswimmers have recently stimulated considerable research interest from experimental [1–6] and theoretical viewpoints [7–9]. This is due to their potential practical applications in lab-on-a-chip devices or drug delivery, and fundamental theoretical significance in non-equilibrium statistical physics and transport processes. Self-phoretic effects have shown to be an effective and promising strategy to design such artificial microswimmers [3–5, 7, 10–12], where the microswimmers are driven by gradient fields locally produced by swimmers themselves in the surrounding solvent. In particular, the collective behavior of a suspension of self-diffusiophoretic swimmers has recently been studied in experiments [13–16].

Self-phoretic swimmers are typically composed of two parts: a functional part which modifies the surrounding solvent properties creating local gradient fields, and a non-functional part which is exposed then to the local field gradients. Most existing experimental investigations of the self-phoretic microswimmers consider Janus particles, which can be quite easily synthesized using partial metal coating on colloidal spheres [3, 5]. In diffusiophoretic microswimmers, the metal coated part catalyzes a chemical reaction to induce a concentration gradient. In thermophoretic microswimmers, the metal coated part is able to effectively absorb heat from e.g. an external laser, which creates a local temperature gradient. The investigations performed by computer simulations have

mostly considered dimer structures composed of two connected beads instead of Janus particles [17–20]. This is motivated by the simplicity of the structure which can be approached by a two beads model. Janus particles have been recently simulated by employing a many beads model [21, 22], which has provided an interesting but computationally costly approach. The fundamental differences on the hydrodynamic behavior of Janus and dimer swimmers, as well as the interest in the investigation of collective phenomena of these systems strongly motivates the development of simple and effective models to simulate the self-phoretic Janus particles.

A single-bead model of the self-phoretic Janus particle in solution is here proposed, together with a detailed comparative study of the hydrodynamic properties of dilute solutions of both self-phoretic Janus particle and microdimer. While the solvent is explicitly described by a coarse grained approach known as multiparticle collision dynamics (MPC), it is necessary to develop a description of a colloidal particle able to produce strong phoretic effect, and reproduce the correct rotational dynamics. The proposed colloid model combines potential interactions with the solvent with stick hydrodynamic boundary conditions, such that integrate the above two properties into a single bead. The properties of self-phoretic Janus particles are introduced then with asymmetric and specific particle surface. The validity of the model is proved by implementing the simulations of both the self-diffusiophoretic and self-thermophoretic microswimmers. The flow field induced by the self-phoretic Janus particle is measured and compared with that around the self-phoretic dimer and their analytical predictions. The efficiency of the model and the consistency of the results puts this method forward as a reliable and powerful tool to investigate the collective behavior of self-phoretic mi-

\*Electronic address: mcyang@iphy.ac.cn

†Electronic address: m.ripoll@fz-juelich.de

crosswimmers.

## II. SIMULATION OF A JANUS MICROSWIMMER IN SOLUTION

The typical sizes and time scales of a Janus colloidal particle and the surrounding solvent particles are separated by several orders of magnitude which are impossible to cover with a microscopic description. Over the last decades various mesoscopic simulation methods have been developed to bridge such an enormous gap. Here, we employ an especially convenient hybrid scheme that describes the solvent by MPC which is a coarse-grained particle-based method [23–28], while the interactions of the Janus particle with the solvent are simulated by standard molecular dynamics (MD).

MPC consists of alternating streaming and collision steps. In the streaming step, the solvent particles of mass  $m$  move ballistically for a time  $h$ . In the collision step, particles are sorted into a cubic lattice with cells of size  $a$ , and their velocities relative to the center-of-mass velocity of each cell are rotated around a random axis by an angle  $\alpha$ . In each collision, mass, momentum, and energy are locally conserved. This allows the algorithm to properly capture hydrodynamic interactions, thermal fluctuations, to account for heat transport and to maintain temperature inhomogeneities [29, 30]. Simulation units are chosen to be  $m = 1$ ,  $a = 1$  and  $k_B \bar{T} = 1$ , where  $k_B$  is the Boltzmann constant and  $\bar{T}$  the average system temperature. Time and velocity are consequently scaled with  $(ma^2/k_B \bar{T})^{1/2}$  and  $(k_B \bar{T}/m)^{1/2}$  respectively. The solvent transport properties are determined by the MPC parameters [31, 32]. Here, we employ the standard MPC parameters  $\alpha = 120^\circ$ ,  $h = 0.1$ , and the mean number of solvent particles per cell  $\rho = 10$ , which corresponds to a solvent with a Schmidt number  $Sc = 13$ . The simulation system is a cubic box of size  $L = 30a$  with periodic boundary conditions.

By construction, a Janus particle has a well-defined orientation with a corresponding well-defined rotation, and surface properties are different in the two colloid hemispheres. In previous studies of colloid phoresis with MPC [18, 19, 33–35], a central type of interaction such as the Lennard Jones potential has been employed, which does not result in a rotational motion. Other studies of rotational colloidal dynamics [36] have employed MPC with boundary conditions that are in fact thermalized stick conditions since a surface colloidal temperature needs to be imposed. In this work, we first modify existing techniques to construct a specific model that allows us to simulate a colloid with stick boundary conditions together with potential interactions with the solvent that locally conserve not only mass and momentum, but also energy. Then, in order to reproduce the properties of a Janus particle, the spherical colloid is divided in two hemispheres characterized by different interactions with the surrounding solvent. One of this halves (with a polar

angle  $\theta \leq \pi/2$  with respect to a defined colloid axis  $\mathbf{n}$ ) is considered to be the *functional* part, while the other half is the *non-functional* part. The functional part of the Janus particle is where the material has special properties like enabling a chemical reaction (catalytic) or carrying a high temperature due to a larger heat adsorption. The special behavior of the functional part originates local gradients (as of concentration or temperature) which will induce a phoretic force applied to one or both halves of the Janus colloid. In the following sections we introduce first the model for a colloid with stick boundary conditions and a well-defined orientation, and then consecutively the thermophoretic and diffusiophoretic Janus particles.

### A. Passive colloid with stick boundary: simulation model

A colloidal particle with stick boundary conditions will vary its direction of motion randomly. This is caused by the stochastic torque exerted on the particle due to collisions with the solvent. On a coarse grained level, stick boundary conditions can be modeled by the bounce back (BB) collision rule [37, 38], this is by reversing the direction of motion of the solvent particle with respect to the colloidal surface. However, the bounce back rule does not induce significant phoretic effects, such that it is necessary to combine it with a soft potential. Practically, we realize this by defining three interaction regions, as shown in Fig. 1, where  $r$  is the distance between a solvent particle and the center of a colloid. For distances larger than the cutoff radius,  $r > r_c$ , there is no interaction. For  $r_b > r > r_c$  just the soft central potential is considered. And for  $r < r_b$ , both the soft potential and the bounce back collision are taken into account. The value of the *bounce-back radius*  $r_b$  should be large enough to ensure that a certain amount of solvent particles participate in the bounce-back collision such that a significant rotational friction is induced. On the other hand, the value of  $r_b$  should also be small enough such that the colloid-solvent potential effectively contribute to the phoretic force.

The interaction potential employed in this work is of Lennard-Jones (LJ) type [39], with the general form

$$U(r) = 4\epsilon \left[ \left( \frac{\sigma}{r} \right)^{2k} - \left( \frac{\sigma}{r} \right)^k \right] + C, \quad r \leq r_c. \quad (1)$$

The positive integer  $k$  controls the stiffness of the potential, and  $r_c$  is the potential cutoff radius. The potential intensity is chosen as one of the system units  $\epsilon = k_B \bar{T} = 1$ , and the interaction length parameter as  $\sigma = 2.5a$ . In this work we choose  $r_b = \sigma$  which is also a good estimation for the colloid radius. Attractive interactions are obtained with  $C = 0$ , and  $r_c = 2.5\sigma$  and repulsive with  $C = \epsilon$  and  $r_c = 2^{1/k}\sigma$ . The mass of the colloidal particle is set to  $M = 4\pi\sigma^3 m\rho/3 = 650m$ , such that the colloid is neutrally buoyant. Between two MPC

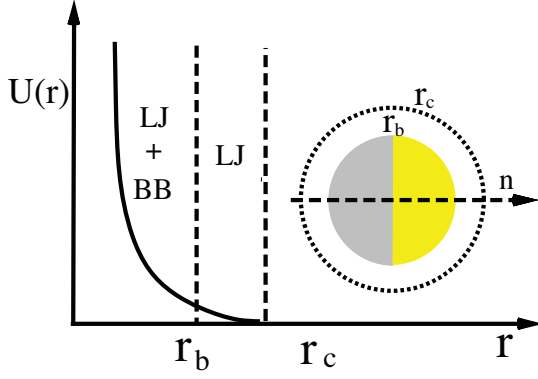


FIG. 1: Schematic diagram of the three regions of the colloid-solvent interactions. The inset is a sketch of a Janus particle.

collision steps,  $N_{md}$  molecular dynamics steps are employed. The equations of motion are integrated by the velocity-Verlet algorithm with a time step  $\Delta t = h/N_{md}$ , where we use  $N_{md} = 50$ .

Mostly bounce-back collision considers the interaction between solvent particles and immobile planar walls, where the particle velocity is simply reversed. Here in contrast, an elastic collision is performed when a point-like solvent particle with velocity  $\mathbf{v}$  is moving towards the spherical colloid and is closer to it than  $r_b$ , this is  $r < r_b$ . The colloidal particle has a linear velocity  $\mathbf{V}$ , an angular velocity  $\omega$ , and a moment of inertia  $I = \chi M \sigma^2$ , with  $\chi = 2/5$  the gyration ratio. Since the collision is now performed with a moving object, the relevant quantity for the collision is  $\tilde{\mathbf{v}}$ , namely, the solvent particle velocity relative to the colloid at the colliding point,

$$\tilde{\mathbf{v}} = \mathbf{v} - \mathbf{V} - \omega \times \mathbf{s}, \quad (2)$$

where  $\mathbf{s} = \mathbf{r} - \mathbf{R}$ , with  $\mathbf{r}$  and  $\mathbf{R}$ , the position of the solvent particle and of the center of the colloid, respectively. In the following, we refer to  $\mathbf{s}$  as the contact vector and  $\tilde{\mathbf{v}}$  as the contact velocity. The conservation of linear and angular momentum imposes the following explicit expressions for the post-collision velocities

$$\begin{aligned} \mathbf{v}' &= \mathbf{v} - \mathbf{p}/m, \\ \mathbf{V}' &= \mathbf{V} + \mathbf{p}/M, \\ \omega' &= \omega + (\mathbf{s} \times \mathbf{p})/I. \end{aligned} \quad (3)$$

The precise form of the momentum exchange  $\mathbf{p}$  can be calculated in terms of the normal and tangential components of the contact velocity  $\tilde{\mathbf{v}}_n = \hat{\mathbf{s}}(\hat{\mathbf{s}} \cdot \tilde{\mathbf{v}})$ , and  $\tilde{\mathbf{v}}_t = \tilde{\mathbf{v}} - \tilde{\mathbf{v}}_n$ , with  $\hat{\mathbf{s}} = \mathbf{s}/|\mathbf{s}|$  the unit contact vector. Imposing the conservation of kinetic energy and stick boundary condition (see calculation details in the Appendix A) leads to  $\tilde{\mathbf{v}}'_n = -\tilde{\mathbf{v}}_n$  and  $\tilde{\mathbf{v}}'_t = -\tilde{\mathbf{v}}_t$ , which determines

$$\mathbf{p} = \mathbf{p}_n + \mathbf{p}_t = 2\mu\tilde{\mathbf{v}}_n + \frac{2\mu\chi M}{\chi M + \mu}\tilde{\mathbf{v}}_t, \quad (4)$$

where  $\mu = mM/(m + M)$  is the reduced mass. This collision rule is similar to the one used in rough hard sphere

systems [40, 41], although in the present case the colliding pair is composed of a point particle and a rough hard sphere [42]. This collision method does not change the positions of the particles and, consequently, the potential energy does not vary discontinuously.

### B. Passive colloid with stick boundary: simulation results

In order to test the correct rotational dynamics of the proposed model, we first verify the exponential decay of the orientational time-correlation function. This is expected to be [43],

$$\langle \mathbf{n}(t) \cdot \mathbf{n}(0) \rangle = \exp(-2D_r t), \quad (5)$$

with the body-fixed orientation vector  $\mathbf{n}$ , and  $D_r$  the rotational diffusion constant. A repulsive potential with  $k = 24$  in Eq. (1) is chosen for the colloid-solvent interactions. A fit of Eq. (5) to our data (shown in Fig. 2) yields  $D_r = 0.0015$  in units of  $(k_B T / m a^2)^{1/2}$ . In order to provide an analytical estimation of this coefficient, it should be taken into account that within the cut-off-radius, the number density of the solvent particles obeys  $\rho(r) = \rho e^{-U(r)/k_B T}$  due to the ideal gas equation of state of the MPC solvent. This results into a position-dependent viscosity. In the following, we refer to the local number density at the colloid surface as  $\rho_\sigma = \rho(\sigma) = \rho e^{-1}$ . The corresponding dynamic and kinematic viscosity at the particle surface are obtained using the dependence of  $\eta$  on  $\rho$  from the kinetic theory [32]. For the MPC solvent employed parameters, we have that  $\eta = 7.93$ ,  $\eta_\sigma = 2.47$  and  $\nu_\sigma = 0.67$ . The Stokes-Einstein equation for the rotational diffusion provides the dependence  $D_r = k_B T / \zeta_H$ , with the hydrodynamic rotational friction  $\zeta_H = 8\pi\eta_\sigma\sigma^3$ . With this approximation, we obtain  $D_r = 0.001$ , which underestimates, but it is still consistent with the simulation result.

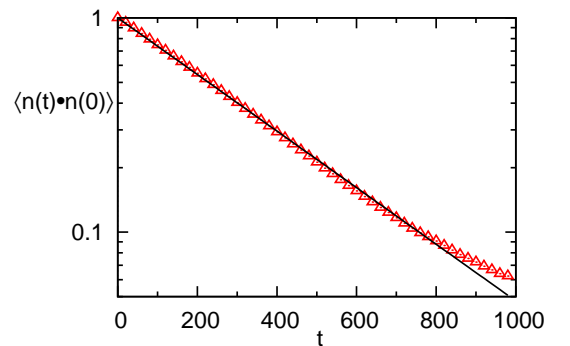


FIG. 2: Time auto-correlation function of the orientation vector of passive colloidal sphere. Symbols refer to simulation results, and the line to Eq. (5).

The rotation dynamics can be further analyzed by measuring the angular velocity autocorrelation function

of the colloidal particle. For short times, Enskog kinetic theory [36, 44] predicts that the autocorrelation function follows a exponential decay,

$$\lim_{t \rightarrow 0} \langle \omega(t) \cdot \omega(0) \rangle = \langle \omega^2 \rangle \exp(-\zeta_E t / I), \quad (6)$$

with  $\langle \omega^2 \rangle = 3k_B T / I$ , as obtained from energy equipartition theorem, and  $\zeta_E$  the Enskog rotational friction coefficient of a sphere suspended in bath of point-like particles [42],

$$\zeta_E = \frac{8}{3} \sqrt{2\pi k_B T \mu \rho_\sigma \sigma^4} \frac{\chi M}{\mu + \chi M}. \quad (7)$$

For long times, the relaxation of the correlation function is predicted by hydrodynamic mode-coupling theory [36, 45] to decay algebraically,

$$\lim_{t \rightarrow \infty} \langle \omega(t) \cdot \omega(0) \rangle = \frac{3\pi k_B T}{m\rho_\sigma (4\pi\nu_\sigma t)^{5/2}}. \quad (8)$$

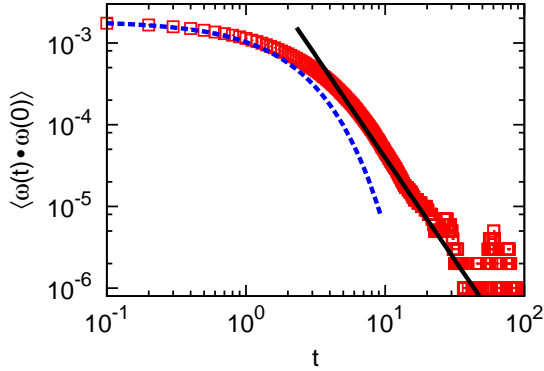


FIG. 3: Time decay of the angular velocity autocorrelation function of passive colloidal sphere. Symbols correspond to simulation results, the dashed line to short-time Enskog prediction in Eq. (6) and solid line to the long-time hydrodynamic prediction in Eq. (8).

The angular velocity autocorrelation function obtained from simulations is displayed in Fig. 3 agrees very well with the theoretical predictions at short and long time regimes respectively in Eq. (6) and (8), where no adjustable parameter is employed. On the other hand, the rotational diffusion coefficient can be understood to be determined by the total friction  $\zeta$ , with  $1/\zeta = 1/\zeta_H + 1/\zeta_E$ . Considering both terms, the analytical prediction is  $D_r = k_B T / \zeta = 0.002$ , which overestimates then the measured value of  $D_r$ . More rigorous expression for the hydrodynamic rotational diffusion coefficient can in principle be obtained by solving the Stokes equation with an inhomogeneous viscosity profile [46].

In conclusion, these results ensure that the coarse-graining model introduced here describes physically correct rotational dynamics where no surface thermalization has been employed. This is the basic colloid model on which the Janus structure can be further introduced.

### C. Self-thermophoretic Janus colloid

A Janus particle partially made/coated with a material of high heat absorption and heated, for example with a laser, develops around it an inhomogeneous temperature distribution [5]. The part of the Janus particle with lower heat absorption is therefore exposed to a solvent with a temperature gradient, which originates a thermophoretic force. Depending on the nature (thermophilic/thermophobic) of the colloid-solvent interactions in the non-functional part of the colloid, the thrust will be exerted towards or against the temperature gradient.

The simulation model combines now the rotating colloid introduced in the preceding section, with elements of the previously investigated self-thermophoretic dimer [19]. In particular, the temperature around the heated hemisphere is fixed by rescaling the thermal energy of the solvent particles closer than  $1.08\sigma$  to the center of the sphere to a value  $T_h$ . This means that only a small layer ( $\simeq 0.08\sigma$ ) around the heated part of the Janus particle is affected by the rescaling. In this work we have restricted ourselves to  $T_h = 1.25\bar{T}$ , although a large range of possible values is accessible. The inserted energy is drained from the system by thermalizing the mean temperature of the system to a fixed value  $\bar{T}$ . In experiments, the thermalization is performed at the system boundaries. Although these two thermalizations are intrinsically different, the differences are expected to be negligible, when the system is large enough, and especially when considering the neighborhood of the Janus particle.

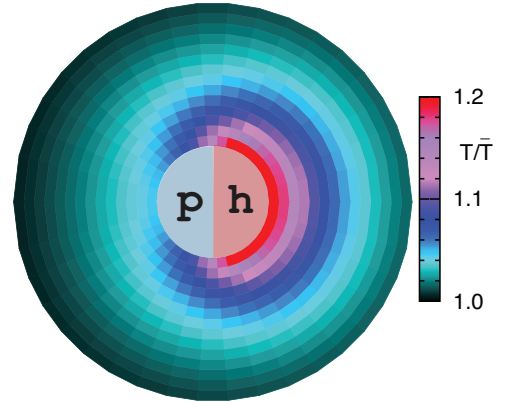


FIG. 4: Temperature distribution induced by a self-thermophoretic Janus particle. Here, the Janus particle has a repulsive LJ potential with  $k = 3$ . The right (h) and the left (p) hemisphere correspond to the heated and the phoretic parts, respectively. Because of axis-symmetry, only the distribution in a section across the axis is displayed.

Two different colloid-solvent potentials of LJ-type Eq. (1) are employed in the simulations provided here, a soft repulsive potential with  $k = 3$ , and a short-range attractive potential with  $k = 24$ . The particular shape of



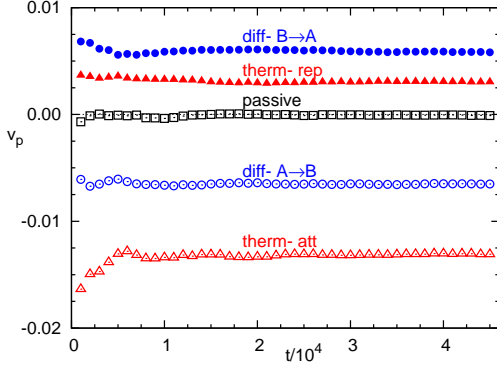


FIG. 5: Self-propelled velocity as a function of time as averaging parameter. Triangles refer to self-thermophoretic Janus particles with repulsive and attractive LJ-type potentials. Circles refer to self-diffusiophoretic Janus particles. Solid symbols refer to forward motion, namely along the polar axis towards the functional part. Open symbols refer to backwards motion. For reference, squares denote the velocity measured for a purely passive colloid.

the colloid-solvent potential has already shown [19, 34] to influence the magnitude of the thermophoretic force, and interestingly also its direction. The repulsive LJ potential is expected to produce a thrust pointing to the heated hemisphere; while the attractive potential will lead to a driving force in the opposite direction. Two procedures are employed to quantify the self-propelled velocity  $v_p$ . A direct characterization can be performed by projecting the center-of-mass velocity of the Janus particle on its polar axis,  $v_p = \langle \mathbf{V} \cdot \mathbf{n} \rangle$ . Figure 5 shows how direct measurements of  $v_p$  are well-defined for different interaction potentials as a function of time, which is employed as an averaging parameter. Indirect determination of  $v_p$  is obtained by measuring the mean square displacement (MSD) of the Janus particle along its polar axis. In this direction, the motion of the Janus particle can be divided into a pure diffusion and a pure drift, and it is related to the self-propelled velocity via

$$\langle (\Delta x_p)^2 \rangle = 2D_p t + v_p^2 t^2. \quad (9)$$

Here  $D_p$  is the translational diffusion coefficient of the Janus particle along its axis. The mean square displacement in the polar direction is shown in Fig. 6 as a function of time for Janus particles with different colloid-solvent interactions. At very small times, an initial inertial regime with a quadratic time dependence is observed. For times larger than the Brownian time, the diffusive behavior coexists with the presence of the self-propelled velocity as indicated in Eq. (9). A fit to the data allows us to determine both  $D_p$  and  $v_p$  with good accuracy. Direct and indirect determination of  $v_p$  agree very well within the statistical accuracy, as can be seen in Table I.

The quantitative values of the propelled velocities are determined by the nature of the thermophoretic forces. As in the case of thermophoretic microdimers [19], these forces are related to the temperature gradients

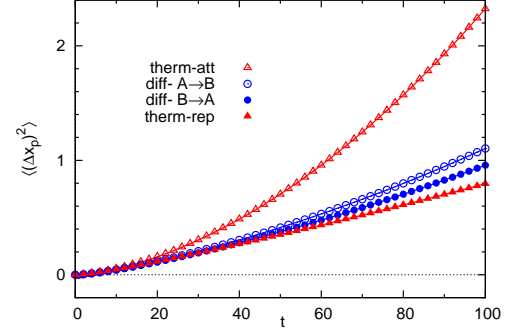


FIG. 6: MSD of the center-of-mass of the Janus particle along the polar axis as a function of time. Simulation parameters are those of Fig. 5. Lines correspond to fits with Eq. (9).

	therm-att	therm-rep	diff-A $\rightarrow$ B	diff-B $\rightarrow$ A
$v_p$ (direct)	-0.0131	0.0030	-0.0065	0.0059
$v_p$ (indirect)	-0.0133	0.0035	-0.0070	0.0059
$D_p$ (indirect)	0.0029	0.0035	0.0032	0.0032
$v_p$ (dimer)	-0.0068	0.0047		
$D_p$ (dimer)	0.0028	0.0034		

TABLE I: Summary of the self-propelled velocities, and the diffusion coefficient of the thermophoretic and diffusiophoretic Janus particles obtained from the simulations with the direct and indirect methods. For comparison the same quantities are displayed for our prior results on the thermophoretic microdimers [19].

$\nabla T$ , and the thermal diffusion factor  $\alpha_T$  which characterizes the particularities of the colloid-solvent interactions [34, 47, 48]. The self-propelled velocity is then  $v_p = -\alpha_T \nabla k_B T / \gamma_p$ , with  $\gamma_p$  the particle translational frictional coefficient and  $D_p = k_B T / \gamma_p$ . The hydrodynamic translational frictional coefficient is  $\gamma_p^H = B \eta \sigma$  with  $B$  being a numerical factor given by the boundary conditions. Colloids with stick boundary conditions have  $B = 6\pi$ , while colloids with slip boundary conditions have  $B = 4\pi$ . The here proposed model provides stick boundary conditions for colloids at  $r \simeq r_b$  with the surface viscosity  $\eta_\sigma$ , and slip for  $r > r_b$ , which means that the overall colloid behavior will be effectively *partial slip*. The stick boundary approach predicts  $k_B T / (6\pi \eta \sigma) \simeq 0.0027$ , such that the slightly larger simulation results in Table I are consistent with the partial slip prediction. In principle these values should still be corrected by considering the Enskog contribution and finite size effects. However, the precise form and validity of these corrections is still under debate for colloids simulated with MPC [26, 42]. It can be observed that the values for the thermophoretic attractive potential are smaller than those for the repulsive one, which reflects the larger viscosity  $\eta_\sigma$  provided by the attractive surface interactions. Interestingly, the values for  $D_p$  of the thermophoretic dimers are very similar than those of the Janus particles. This can be understood as the

result of two canceling effects. On the one hand the microdimer has larger size than the Janus particle, which decreases the translational diffusion. On the other hand, the microdimer is here simulated with slip boundary conditions, which reduces the friction in comparison with the stick, or partial slip boundary conditions employed for the Janus particle. Given that  $D_p$  is not significantly changing for the results in Table I, the variation of numerical values of  $v_p$  can be related to the differences in  $\nabla T$  and  $\alpha_T$ . The actual value of  $\nabla T$  varies along the particle surface, and it is not the same for both particle geometries. The determination of  $\alpha_T$  is given by the size, the geometry, and the specific interactions between the colloid and the solvent. The comparison of the measured  $v_p$  for the dimer and the Janus particles is therefore non-trivial and deserves a more in-depth investigation. Furthermore, the bounce-back surface considered in the Janus particle model produces an additional thermophobic thrust, which could explain the enhanced value of the Janus particle with attractive interactions.

In the presence of a temperature gradient, the transport of heat is a relevant process which in experimental systems occurs in a much faster time scale than the particle thermophoresis [5, 49, 50]. For thermal energy propagation the characteristic time is  $\tau_\kappa \sim a^2/\kappa$  with  $\kappa$  the thermal diffusivity, and the time scale of particle motion is related to the self-propelled velocity by  $\tau_m \sim a/v_p$ . Using  $\kappa$  estimated from kinetic theory [32] and the measured  $v_p$ , we have  $\tau_\kappa/\tau_m \sim 10^{-1}$  for our simulation parameters. This means that both times are also well-separated in the simulations, and that temperature profile around the swimmer is almost time-independent.

#### D. Self-diffusiophoretic Janus colloid

A colloidal particle with a well-defined part of its surface with catalytic properties can display self-propelled motion [1, 3, 13, 14, 51]. Such functional or catalytic part of the Janus particle catalyzes a chemical reaction, which creates a surrounding concentration gradient of the solvent components involved in the reaction, which typically have different interactions with the colloid. This gradient in turn induces a mechanical driving force (diffusiophoretic force) on the Janus particle and hence propulsion. The direction of the self-propelled motion will be related to the interaction of each solvent component with the colloid. Chemical reactions are generally accompanied by an adsorption or emission of energy. A catalytic Janus particle could therefore generate a local temperature gradient which would induce an additional thermophoretic thrust. However, existing experiments of Pt-Au micro-rods [1] have shown the contribution of this effect to be negligible.

The effect of irreversible chemical reactions has already been included in a MPC simulation study of chemically powered nanodimers by Rückner and Kapral [17]. Similar to that work, we here consider a solvent with two

species A and B, together with the model of the stick boundary colloid previously introduced. The reaction  $A \rightarrow B$  is performed with a probability  $p_R$  whenever an A-solvent particle is closer than a distance  $r_1$  to the catalytic hemisphere of the Janus particle (see inset of Fig. 7). Besides this reaction and the MPC collision, there are no further interactions between A and B solvent particles. Another important element to induce self-propelled motion is that the interaction of each component with the colloid surface should be different [17]. We therefore consider that solvent species A and B interact with the Janus particle with different potentials  $U_A(r)$  and  $U_B(r)$ , but with the same bounce-back rule. A change of potential energy at the point where the  $A \rightarrow B$  reaction occurs could be numerically unstable, and would lead to a local heating or cooling of the surrounding solvent. In order to model here a purely diffusiophoretic swimmer, we choose smoothly varying potentials  $U_A(r)$  and  $U_B(r)$  which completely overlap for  $r \leq r_1$ , ensuring a reaction without an energy jump. We consider  $U_B(r)$  as the repulsive LJ-type potential in Eq. (1) with  $k = 12$ .  $U_A(r)$  in Fig. 7 is constructed in four intervals by a cubic spline interpolation, which yields to

$$U_A(r) = \begin{cases} U_B(r) & (r \leq r_1) \\ a_0 + a_1 r + a_2 r^2 + a_3 r^3 & (r_1 \leq r \leq r_2) \\ b_0 + b_1 r + b_2 r^2 + b_3 r^3 & (r_2 \leq r \leq r_3) \\ 0 & (r_3 \leq r) \end{cases} \quad (10)$$

where the coefficients and the distances to determine the related intervals are specified in the Table II.

$a_0 = 844.6$	$a_1 = -849.7$	$a_2 = 280.7$	$a_3 = -30.3$
$b_0 = 3283$	$b_1 = -3610$	$b_2 = 1322$	$b_3 = -161.4$
$r_b = \sigma$	$r_1 = 1.0132\sigma$	$r_2 = 1.06\sigma$	$r_3 = 1.12\sigma$

TABLE II: Coefficients employed in the simulations for the potential function  $U_A$  in Eq. (10).

Simulations are initiated with a solvent composed only of A-type particles. The considered chemical reaction  $A \rightarrow B$  in the catalytic part of the Janus particle is irreversible, such that A-type solvent particles are gradually consumed. In order to keep a stationary concentration gradient, A-particles are constantly fed into the system. Concretely, we fix the reaction probability to  $p_R = 0.1$ , and whenever a B-type particle is at a distance  $d$  from the Janus particle (we consider  $d = 5\sigma$ ), it automatically converts into A. This allows the system to reach an steady-state concentration distribution of B molecules around the swimmer. Figure 8 shows  $\rho_B$ , the number of B-type particles per unit cell. It can be seen that on the catalytic hemisphere there are mostly B-type particles, while in the phoretic hemisphere the situation is reversed and there are mostly A-particles. The self-propelled velocity is quantified by using the direct and indirect methods as already described for the self-thermophoretic Janus particles. The results are displayed separately in Fig. 5

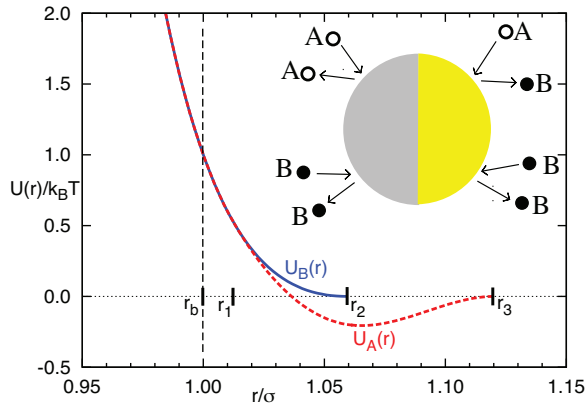


FIG. 7: Potential interactions between the two solvent species and the Janus particle.  $U_A(r)$  is defined in Eq. (10) and  $U_B(r)$  in Eq. (1). Inset: Schematic representation of the catalytic and non-catalytic hemispheres of the Janus particle and the interaction of the A and B species with each hemisphere.

and Fig. 6, and the numerical values are summarized in Table I where the nice agreement between the methods can be observed. The diffusion coefficients for the both diffusiophoretic Janus particles are the same, which is related to the fact that at the surface both potentials are the same. The value of the self-propulsion velocity,  $v_p$ , is determined by the choice of the colloid-solvent potentials, the reaction probability and the boundary conditions. For the considered  $A \rightarrow B$  reaction with  $U_B(r)$  repulsive, and  $U_A(r)$  attractive, the concentration gradient pushes the Janus particle against the direction of the polar axis  $\mathbf{n}$ . A reciprocal choice of potentials, which is almost equivalent to consider the reaction  $B \rightarrow A$ , pushes the Janus particle along  $\mathbf{n}$  as can be verified in Fig. 5 and Table I. It should be noted that the values of the velocities in both simulations are not exactly reversed, since the reciprocal choice of potentials does not correspond to a perfectly reverse distribution of the species concentrations. A comparison of the velocities for the diffusiophoretic Janus particle in this work, and the existing data for microdimers and Janus particles [17, 22] is not really straightforward since the employed parameters and potentials are different. The systems are though not so different, and the values of  $v_p$  range from similar values to approximately four times smaller.

The time scale of the particle motion of a self-diffusiophoretic swimmer  $\tau_m$  needs to be compared with the time scale of solvent molecule diffusion  $\tau_s$ , which is a much faster process in experimental systems. The solvent diffusion coefficient  $D_s$  determines  $\tau_s = a^2/D_s$ . For the employed simulation parameters,  $D_s$  from the kinetic theory, and the measured  $v_p$  determine the separation of both time scales to be  $\tau_s/\tau_m \sim 10^{-1}$ .

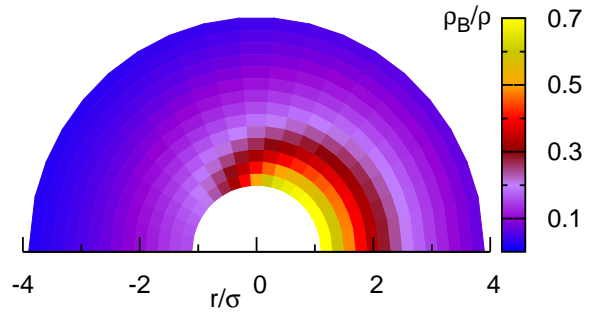


FIG. 8: Local number density distribution of B-type particles induced by a self-diffusiophoretic Janus particle with the  $A \rightarrow B$  reaction. The right hemisphere corresponds to the catalytic part.

### III. FLOW FIELD AROUND PHORETIC SWIMMERS

In the previous section, an efficient model to simulate the behavior of self-phoretic Janus particles has been introduced, and the obtained velocities have been related with the employed system parameters. Another fundamental aspect in the investigation of microswimmers is the effect of hydrodynamic interactions [52], and how do these compare with the effect of concentration or temperature gradients. In the case of self-propelled particles, the temperature or concentration distributions decay with  $1/r$  around the particle, such that their gradients decay as  $1/r^2$ . Furthermore, the hydrodynamic interactions have shown to be fundamentally different for swimmers of various geometries and propulsion mechanisms, yielding to phenomenologically different behaviors classified in three types, pullers, pushers, and neutral swimmers [52]. In the following, we investigate the solvent velocity fields generated by the self-phoretic Janus particles, as well as those generated by self-phoretic microdimers, and in both cases the analytical predictions are compared with simulation results. The velocity field around a self-propelled particle can be analytically calculated from the Navier-Stokes equation. Here, we solve the Stokes equation, which neglects the effect of inertia due to very small Reynolds number, and consider the incompressible fluid condition [10, 35]. Note that although MPC has the equation of state of an ideal gas, the compressibility effects of the associated flow fields have shown to be very small in the case of thermophoretic particles [35]. We also implicitly assume that the standard boundary layer approximation is valid, this is that the particle-solvent interactions are short-ranged. In order to solve the Stokes equation, three hydrodynamic boundary conditions need to be determined. In the particle reference frame the normal component of the flow field at the particle surface vanishes. Considering sufficiently large systems, it is reasonable to assume vanishing velocity field at infinity. Finally, the integral of the stress tensor over the particle surface has to be identified in each geometry.

### A. Self-phoretic Janus particle

For a self-phoretic Janus particle, the propulsion force balances with the friction force due to the particle motion, such that the integral of stress tensor over the particle surface vanishes. The resulting velocity field reads

$$\mathbf{v}(\mathbf{r}) = \frac{\sigma^3}{2r^3} \left( 3 \frac{\mathbf{r}\mathbf{r}}{r^2} - \mathbf{I} \right) \cdot \mathbf{v}_p, \quad (11)$$

with  $\mathbf{I}$  the unit tensor,  $\mathbf{r}$  the distance to the colloid center, and  $r = |\mathbf{r}|$ . Note that the boundary conditions are the same as in the case of a thermophoretic particle moving in an external temperature gradient and therefore also the velocity field [35]. Equation (11) indicates that the velocity field is a source dipole, which decays fast with the distance as  $1/r^3$ . It is therefore to be expected that in suspensions of the self-phoretic Janus particles, the hydrodynamic interactions are negligible in comparison to the effects of concentration or temperature gradients.

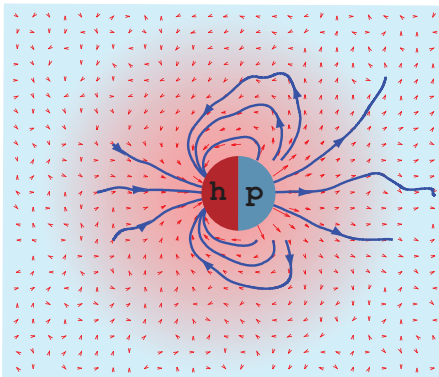


FIG. 9: Velocity field induced by a self-thermophoretic Janus particle with a thermophobic surface. The left (h) and the right (p) hemisphere corresponds to the heated and the phoretic part, respectively. Propulsion and flow field on the axis  $\mathbf{n}$  point in the same direction. Small arrows represents the flow velocity magnitude and direction, and lines refer to the streamlines of the flow field. The background color code does not precisely correspond to the temperature distribution, and should be taken as a guide to the eye.

Direct measurements of the flow field around the microswimmers can be performed in the simulations and allow a quantitative comparison with the analytical expression. Since only small differences are expected between the two discussed types of phoretic swimmers, we focus in the following on the thermophoretic microswimmers. Figure 9 shows the velocity field induced by a self-thermophoretic Janus particle with a thermophobic surface in a section across the particle center. The measured velocity field has a source-dipole type pattern, in which propulsion and flow field along the particle axis have the same direction as expected from the analytical prediction in Eq. (11). The quantitative values of the simulated velocity fields are compared with the analytical predictions in Fig. 10 for both the self-thermophoretic and the self-diffusiophoretic Janus particle. The flow field component

along the Janus particle axis,  $\mathbf{v} \cdot \mathbf{n}$ , is displayed along the Janus particle axis  $\mathbf{n}$  in Fig. 10 a and perpendicular to it in Fig. 10 b. Simulation results and analytical predictions are in very good agreement without any adjustable parameter, although on the axis perpendicular to  $\mathbf{n}$  the theory slightly underestimates the velocity field of the self-thermophoretic Janus particle at short distances. The underestimation probably arises from the sharp change of the solvent properties at the border between the functional and non-functional hemispheres [53], which is disregarded in the present analytical calculation.

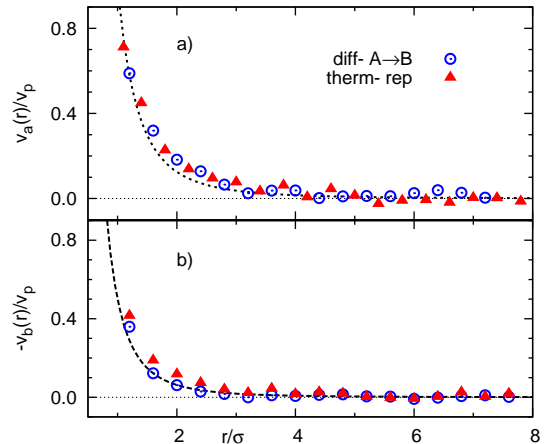


FIG. 10: Rescaled flow velocity,  $\mathbf{v} \cdot \mathbf{n}$ , as a function of the distance to the center of the Janus particle (positive direction towards the functional part). Symbols refer to the simulation results, and lines to the predictions in Eq. (11). a) Velocity along the axis  $\mathbf{n}$ . b) Velocity along the axis perpendicular to  $\mathbf{n}$ .

### B. Self-phoretic microdimer

Besides the Janus particle, other particle geometries have been shown to be easy to construct phoretic swimmers. Such an alternative is the microdimer [17, 19], composed of two strongly attached beads, in which one bead acts as the functional end, and the other bead as the non-functional one. The Stokes equation can be solved independently for each bead, and the total velocity field around the self-propelled microdimer can be approximated as a superposition of these two velocity fields. The dimer is a typical force dipole such that integral of stress tensor over each bead is non-zero, although their sum vanishes. This is fundamentally different from the case of the Janus particle [8, 53]. The integral over the functional bead corresponds to the frictional force, which is associated with the propulsion velocity by  $\gamma v_p$ , with  $\gamma_p$  the friction coefficient. The integral over the non-functional bead corresponds to the driving force which has the same magnitude as the friction force, but opposite direction; this results in zero net force on the dimer.



By solving the Stokes equation, the velocity field produced by the functional and non-functional beads are

$$\mathbf{v}_f(\mathbf{r}) = \frac{\sigma}{2|\mathbf{r} - \mathbf{r}_f|} \left( \frac{(\mathbf{r} - \mathbf{r}_f)(\mathbf{r} - \mathbf{r}_f)}{|\mathbf{r} - \mathbf{r}_f|^2} + \mathbf{I} \right) \cdot \mathbf{v}_p, \quad (12)$$

and

$$\begin{aligned} \mathbf{v}_{nf}(\mathbf{r}) = & -\frac{\sigma}{2|\mathbf{r} - \mathbf{r}_{nf}|} \left( \frac{(\mathbf{r} - \mathbf{r}_{nf})(\mathbf{r} - \mathbf{r}_{nf})}{|\mathbf{r} - \mathbf{r}_{nf}|^2} + \mathbf{I} \right) \cdot \mathbf{v}_p \\ & + \frac{\sigma^3}{|\mathbf{r} - \mathbf{r}_{nf}|^3} \left( \frac{3(\mathbf{r} - \mathbf{r}_{nf})(\mathbf{r} - \mathbf{r}_{nf})}{|\mathbf{r} - \mathbf{r}_{nf}|^2} - \mathbf{I} \right) \cdot \mathbf{v}_p, \end{aligned} \quad (13)$$

respectively. Here,  $\mathbf{r}_f$  and  $\mathbf{r}_{nf}$  are the position coordinates of the functional and non-functional beads, respectively. Note that the second term on the right side of Eq. (13) corresponds to a source dipole, which arises from the excluded volume effect of the bead (vanishing for point particle). Thus, the total velocity field around the self-propelled microdimer can be approximated by

$$\mathbf{v}(\mathbf{r}) = \mathbf{v}_f(\mathbf{r}) + \mathbf{v}_{nf}(\mathbf{r}) \sim 1/r^2. \quad (14)$$

Consequently, in suspensions composed of phoretic microdimers the hydrodynamic interactions are comparable to the contributions coming from concentration or temperature gradients. Furthermore, the near-field hydrodynamic behaviors of the dimer also differ remarkably from the Janus particle.

Simulations of self-thermophoretic dimers allow us to perform precise measurements of the induced flow field. The simulation model is the same one as employed in our previous work [19] where each bead has a radius  $\sigma = 2.5a$  and the distance between the beads centers is  $d = |\mathbf{r}_{nf} - \mathbf{r}_f| = 5.5a$ . The interactions between the beads and the solvent are of Lennard-Jones type, cf. Eq. (1). The heated bead interacts with the solvent through a repulsive potential ( $C = \epsilon$  and  $k = 24$ ), while for the phoretic bead two different interactions have been chosen, an attractive ( $C = 0$  and  $k = 48$ ) and a repulsive interaction ( $C = \epsilon$  and  $k = 3$ ). The solvent velocity field is computed around the dimer and displayed for dimers with both interaction types in Fig. 11. In spite of the opposite orientations and the difference in intensity, the pattern of the two flow fields are very similar. The velocity field on the axis across the dimer center and perpendicular to the symmetry axis is, for the microdimer with thermophilic interactions (repulsive), oriented towards the dimer center, while for the thermophobic dimer (attractive interactions) is oriented against the dimer center. This is consistent with the well-known hydrodynamic character of force dipoles [52], and has further important consequences. If another dimer or particle is placed lateral and close to the dimer, the flow field will exert certain attraction in the case of a thermophilic microdimer and certain repulsion in the case of a thermophobic microdimer, which allows us to identify them respectively as *pushers* and *pullers*.

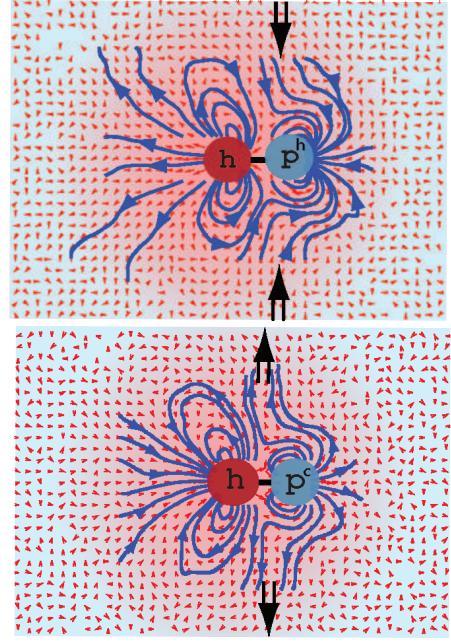


FIG. 11: Solvent velocity field and stream lines induced by self-thermophoretic microdimers. a) Pusher-type of swimmer for a thermophilic microdimer. b) Puller-type of swimmer for a thermophobic microdimer. The left bead (h) corresponds to the heated bead, and the right (p) to the phoretic or propelling one,  $p^h$  stands for thermophilic bead, and  $p^c$  for thermophobic.

A quantitative comparison of the simulated velocity fields with the analytical prediction in Eq. (14) is presented in Fig. 12 for both a pusher- and puller-type microdimer. The flow field component on the microdimer axis analyzed along such axis is displayed in Fig. 12a for the left and right branches. The flow field component perpendicular to the microdimer axis analyzed along such axis is displayed in Fig. 12b. The small deviations along the perpendicular axis are mostly due to statistical errors in the simulations, while those on the bond-axis are slightly larger. This can be attributed to the fact that the superposition approximation in Eq. (14) is less precise in the case of nearby beads. In spite this consideration, Fig. 12 shows in all cases that the analytical solution of the Stokes equation agrees very nicely with the results from the MPC simulations without any adjustable parameter, which constitutes a convincing validation for both the analytical approximations and the model employed in the simulations.

#### IV. CONCLUSIONS

A coarse grained model to simulate a synthetic self-phoretic Janus particle in which hydrodynamic interactions are consistently implemented is here proposed and analyzed. The Janus particle is provided with a proper rotation dynamics through stick particle boundary con-

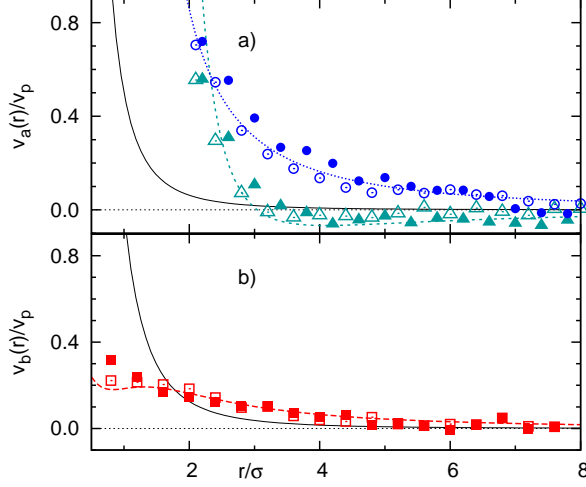


FIG. 12: Rescaled flow velocity as a function of distance to the dimer center of mass. Symbols refer to the simulation results, and discontinuous lines to the theoretical prediction in Eq. (14). Solid symbols regard dimers with a thermophilic bead and a pusher-like behavior. Open symbols regard dimers with a thermophobic bead and a puller-like behavior. For comparison, thin solid lines corresponds to the flow of the Janus particle in Eq. (11). a) Velocity along the dimer axis. Triangles and circles correspond to the velocities on the left and right sides of the dimer center, respectively. b) Velocity perpendicular to the dimer axis, with positive direction pointing to the dimer center.

ditions. These are modeled by bounce-back collisions which reverse the direction of motion of the solvent particle with respect to the moving colloidal surface. The collisions are imposed to conserve linear and angular momentum, as well as kinetic energy. A strong self-phoretic effect is realized by using a soft particle-solvent potential implemented in a larger interaction distance than the bounce-back collisions. With this model both the self-thermophoretic and the self-diffusiophoretic Janus particles are simulated in a straightforward manner, which further justifies the model validity. Simulations to quantify the flow fields induced by the self-phoretic Janus and dimer microswimmers are then also performed, and satisfactorily compared with corresponding analytical predictions. The flow field around the self-phoretic Janus particle shows to be short ranged, as it is typical from neutral swimmers. In contrast, self-phoretic microdimers induce a long-ranged flow field. Dimers propelled towards the functional bead, as thermophilic microdimers, show a hydrodynamic lateral attraction typical from pushers. Conversely, dimers propelled against the functional bead, as thermophobic microdimers, show a hydrodynamic lateral repulsion typical from pullers. These fundamental differences will result in systems with very different collective properties, for which our simulation model is very adequately suited.

## Acknowledgments

M.Y. acknowledges partial support from the “100 talent plan” of Institute of Physics, Chinese Academy of Sciences, China.

## Appendix A: Bounce-back with a moving spherical particle

Considering the contact velocity in Eq. (2) and the post-collision quantities in Eq. (3), the post-collision contact velocity can be calculated as

$$\tilde{\mathbf{v}}' = \tilde{\mathbf{v}} - \frac{\mathbf{p}}{\mu} + \frac{1}{\chi M} [\hat{\mathbf{s}}(\hat{\mathbf{s}} \cdot \mathbf{p}) - \mathbf{p}], \quad (\text{A1})$$

where the relation of the vector triple product with the scalar product has been employed. The difference between the relative pre- and post-collision velocity,  $\Delta \tilde{\mathbf{v}} = \tilde{\mathbf{v}}' - \tilde{\mathbf{v}}$ , can be decomposed into a normal and a tangential component as

$$\Delta \tilde{\mathbf{v}}_n = -\frac{1}{\mu} \hat{\mathbf{s}}(\hat{\mathbf{s}} \cdot \mathbf{p}) \quad (\text{A2})$$

$$\Delta \tilde{\mathbf{v}}_t = [\hat{\mathbf{s}}(\hat{\mathbf{s}} \cdot \mathbf{p}) - \mathbf{p}] \left( \frac{1}{\mu} + \frac{1}{\chi M} \right), \quad (\text{A3})$$

with which  $\mathbf{p}$  can be expressed as

$$\mathbf{p} = \mu \left( \Delta \tilde{\mathbf{v}}_n + \frac{\chi M}{\chi M + \mu} \Delta \tilde{\mathbf{v}}_t \right), \quad (\text{A4})$$

The difference in kinetic energy before and after the collision can be calculated from the pre- and post-collision velocities in Eq. (3) as

$$\Delta E = -2\mathbf{p} \cdot \tilde{\mathbf{v}} + \frac{\mathbf{p}^2}{\mu} + \frac{1}{\chi M} [\mathbf{p}^2 - (\hat{\mathbf{s}} \cdot \mathbf{p})^2], \quad (\text{A5})$$

where the circular shift property of the mixed product has been used. Employing the expression of  $\Delta \tilde{\mathbf{v}}_n$  in Eq. (A2) and of  $\mathbf{p}$  and  $\mathbf{p}^2$  which can be obtained from Eq. (A4), the previous expression can be rewritten as

$$\begin{aligned} \Delta E = & \frac{\mu}{2} (2\tilde{\mathbf{v}} + \Delta \tilde{\mathbf{v}}_n) \cdot \Delta \tilde{\mathbf{v}}_n \\ & + \frac{1}{2} \frac{\chi M}{\chi M + \mu} (2\tilde{\mathbf{v}} + \Delta \tilde{\mathbf{v}}_t) \cdot \Delta \tilde{\mathbf{v}}_t. \end{aligned} \quad (\text{A6})$$

To ensure a collision with energy conservation, it is necessary that both components of the previous expression vanish, since the prefactors are determined by the system under study. Using orthogonality of normal and tangential velocity components the two previous conditions translate into,  $\tilde{\mathbf{v}}_n^2 = \tilde{\mathbf{v}}_n'^2$  and  $\tilde{\mathbf{v}}_t^2 = \tilde{\mathbf{v}}_t'^2$ . Two physical meaningful solutions exist, both with  $\tilde{\mathbf{v}}_n = -\tilde{\mathbf{v}}_n'$ . One is the specular reflection of smooth hard spheres,  $\tilde{\mathbf{v}}_t = \tilde{\mathbf{v}}_t'$ , which is well-known to imply slip-boundary condition. Another solution is the bounce-back reflection of rough

hard spheres,  $\tilde{\mathbf{v}}_t = -\tilde{\mathbf{v}}'_t$ , which enforces a no-slip boundary condition between the solvent and the solute. With both conditions it is possible to express  $\Delta\tilde{\mathbf{v}}$  and hence  $\mathbf{p}$

in terms of the components of the pre-collision contact velocity  $\tilde{\mathbf{v}}$ , which is specified in Eq. (4) for the no-slip condition employed in this work.

- 
- [1] W. F. Paxton, K. C. Kistler, C. C. Olmeda, A. Sen, S. K. S. Angelo, Y. Cao, T. E. Mallouk, P. E. Lammert, and V. H. Crespi, *J. Am. Chem. Soc.* **126**, 13424 (2004).
  - [2] R. Dreyfus, J. Baudry, M. L. Roper, M. Fermigier, H. A. Stone, and J. Bibette, *Nature* **437**, 862 (2005).
  - [3] J. R. Howse, R. A. L. Jones, A. J. Ryan, T. Gough, R. Vafabakhsh, and R. Golestanian, *Phys. Rev. Lett.* **99**, 048102 (2007).
  - [4] L. F. Valadares, Y. G. Tao, N. S. Zacharia, V. Kitaev, F. Galembeck, R. Kapral, and G. A. Ozin, *Small* **6**, 565 (2010).
  - [5] H. R. Jiang, N. Yoshinaga, and M. Sano, *Phys. Rev. Lett.* **105**, 268302 (2010).
  - [6] G. Volpe, I. Buttinoni, D. Vogt, H.-J. Kümmerer, and C. Bechinger, *Soft Matter* **7**, 8810 (2011).
  - [7] R. Golestanian, T. B. Liverpool, and A. Ajdari, *Phys. Rev. Lett.* **94**, 220801 (2005).
  - [8] R. Golestanian, *Phys. Rev. Lett.* **108**, 038303 (2012).
  - [9] B. Sabass and U. Seifert, *J. Chem. Phys.* **136**, 064508 (2012).
  - [10] J. L. Anderson, *Annu. Rev. Fluid Mech.* **21**, 61 (1989).
  - [11] R. Golestanian, T. B. Liverpool, and A. Ajdari, *New J. Phys.* **9**, 126 (2007).
  - [12] J. A. Cohen and R. Golestanian, *Phys. Rev. Lett.* **112**, 068302 (2014).
  - [13] J. Palacci, C. Cottin-Bizonne, C. Ybert, and L. Bocquet, *Phys. Rev. Lett.* **105**, 088304 (2010).
  - [14] I. Theurkauff, C. Cottin-Bizonne, J. Palacci, C. Ybert, and L. Bocquet, *Phys. Rev. Lett.* **108**, 268303 (2012).
  - [15] J. Palacci, S. Sacanna, A. P. Steinberg, D. J. Pine, and P. M. Chaikin, *Science* **339**, 936 (2013).
  - [16] I. Buttinoni, J. Bialké, F. Kümmel, H. Löwen, C. Bechinger, and T. Speck, *Phys. Rev. Lett.* **110**, 238301 (2013).
  - [17] G. Rückner and R. Kapral, *Phys. Rev. Lett.* **98**, 150603 (2007).
  - [18] Y. G. Tao and R. Kapral, *Soft Matter* **6**, 756 (2010).
  - [19] M. Yang and M. Ripoll, *Phys. Rev. E* **84**, 061401 (2011).
  - [20] S. Thakur and R. Kapral, *Phys. Rev. E* **85**, 026121 (2012).
  - [21] F. Lugli, E. Brini, and F. Zerbetto, *J. Chem. Phys.* **116**, 592 (2012).
  - [22] P. de Buyl and R. Kapral, *Nanoscale* **5**, 1337 (2013).
  - [23] A. Malevanets and R. Kapral, *J. Chem. Phys.* **110**, 8605 (1999).
  - [24] A. Malevanets and R. Kapral, *J. Chem. Phys.* **112**, 7260 (2000).
  - [25] M. Ripoll, K. Mussawisade, R. G. Winkler, and G. Gompper, *Phys. Rev. E* **72**, 016701 (2005).
  - [26] J. T. Padding and A. A. Louis, *Phys. Rev. E* **93**, 031402 (2006).
  - [27] R. Kapral, *Adv. Chem. Phys.* **140**, 89 (2008).
  - [28] G. Gompper, T. Ihle, D. M. Kroll, and R. G. Winkler, *Adv. Polym. Sci.* **221**, 1 (2009).
  - [29] D. Lüsebrink and M. Ripoll, *J. Chem. Phys.* **136**, 084106 (2012).
  - [30] M. Yang and M. Ripoll, *Soft Matter* **10**, 1006 (2014).
  - [31] E. Tüzel, M. Strauss, T. Ihle, and D. M. Kroll, *Phys. Rev. E* **68**, 036701 (2003).
  - [32] E. Tüzel, T. Ihle, and D. M. Kroll, *Phys. Rev. E* **74**, 056702 (2006).
  - [33] C. Echevería, K. Tucci, and R. Kapral, *J. Phys.: Condens. Matter* **19**, 065146 (2007).
  - [34] D. Lüsebrink, M. Yang, and M. Ripoll, *J. Phys.: Condens. Matter* **24**, 284132 (2012).
  - [35] M. Yang and M. Ripoll, *Soft Matter* **9**, 4661 (2013).
  - [36] J. T. Padding, A. Wysocki, H. Löwen, and A. A. Louis, *J. Phys.: Condens. Matter* **17**, S3393 (2005).
  - [37] S. Chen and G. D. Doolen, *Annu. Rev. Fluid Mech.* **30**, 329 (1998).
  - [38] A. Lamura, G. Gompper, T. Ihle, and D. M. Kroll, *Europhys. Lett.* **56**, 319 (2001).
  - [39] G. A. Vliegenthart, J. F. M. Lodge, and H. N. W. Lekkerkerker, *Physica A* **263**, 378 (1999).
  - [40] M. P. Allen and D. J. Tildesley, *Computer Simulations in Liquids* (Clarendon, Oxford, 1987).
  - [41] B. J. Berne, *The Journal of Chemical Physics* **66**, 2821 (1977).
  - [42] J. K. Whitmer and E. Luijten, *Journal of Physics: Condensed Matter* **22**, 104106 (2010).
  - [43] M. Doi and S. F. Edwards, *The Theory of Polymer Dynamics* (Oxford University Press, Oxford, 1986).
  - [44] G. Subramanian and H. T. Davis, *Phys. Rev. A* **11**, 1430 (1975).
  - [45] M. H. Ernst, E. H. Hauge, and J. M. J. van Leeuwen, *Phys. Rev. Lett.* **25**, 1254 (1970).
  - [46] D. Rings, D. Chakraborty, and K. Kroy, *New J. Phys.* **14**, 053012 (2012).
  - [47] M. Braibanti, D. Vigolo, and R. Piazza, *Phys. Rev. Lett.* **100**, 108303 (2008).
  - [48] A. Würger, *Rep. Prog. Phys.* **73**, 126601 (2010).
  - [49] S. Wiegand, *J. Phys.: Condens. Matter* **16**, R357 (2004).
  - [50] D. Rings, R. Schachoff, M. Selmke, F. Cichos, and K. Kroy, *Phys. Rev. Lett.* **105**, 090604 (2010).
  - [51] Y. Hong, N. M. K. Blackman, N. D. Kopp, A. Sen, and D. Velegol, *Phys. Rev. Lett.* **99**, 178103 (2007).
  - [52] E. Lauga and T. R. Powers, *Rep. Prog. Phys.* **72**, 096601 (2009).
  - [53] T. Bickel, A. Majee, and A. Würger, *Phys. Rev. E* **88**, 012301 (2013).